Magnetic Resonance in Medicine 57:661–669 (2007)

Functional Imaging With Turbo-CASL: Transit Time and Multislice Imaging Considerations

Gregory R. Lee,* Luis Hernandez-Garcia, and Douglas C. Noll

The optimal use of turbo continuous arterial spin labeling (Turbo-CASL) for functional imaging in the presence of activation-induced transit time (TT) changes was investigated. Functional imaging of a bilateral finger-tapping task showed improved sensitivity for Turbo-CASL as compared to traditional CASL techniques for four of six subjects when scanned at an appropriate repetition time (TR). Both experimental and simulation results suggest that for optimal functional sensitivity with Turbo-CASL, the pulse TR should be set to a value that is 100–200 ms less than the resting-state TT. Simulations were also run to demonstrate the differences in TT sensitivity of different slices within a multislice acquisition, and the signal loss that is expected as the number of slices is increased. Despite the lower baseline ASL signal provided by the Turbo-CASL acquisition, one can achieve equal or improved functional sensitivity due in part to the signal enhancement that accompanies the decrease in TT upon activation. Turbo-CASL is thus a promising technique for functional ASL at higher temporal resolution. Magn Reson Med 57:661–669, 2007. © 2007 Wiley-Liss, Inc.

Key words: arterial spin labeling; fMRI; Turbo-ASL; transit time; CBF; perfusion

Arterial spin labeling (ASL) techniques use blood as an endogenous tracer to image perfusion (1). This requires subtraction of a control image from a labeled image to form a perfusion-weighted image. ASL has a number of benefits that make it attractive as a functional imaging technique. As a cerebral blood flow (CBF) measurement, the ASL signal is more meaningful physiologically than the blood oxygen level-dependent (BOLD) signal, which arises from a complex interplay of parameters (CBF, cerebral blood volume, hematocrit, etc.). Recent studies have also indicated that the ASL signal may be better localized than the BOLD signal (2). Despite these advantages, however, widespread adoption of ASL as a functional imaging technique has been hampered by its lower signal-to-noise ratio (SNR) and temporal resolution. The need to build up a significant amount of label, and the use of a pairwise image acquisition result in low temporal resolution. It is desirable to preserve the pairwise acquisition scheme because of its insensitivity to field drift and thus improved application to low-frequency paradigms (3).

Recently, a couple of methods for acquiring ASL perfusion images at a greatly reduced TR compared to traditional schemes have been introduced (4,5). The common feature of these "turbo" methods is that spins are tagged for a shorter period of time, such that a control image can be acquired immediately after labeling and before any tag has arrived at the imaging slice. The tag then reaches the slice the following TR, during which the tag image is acquired. These techniques can be used to map functional activations at a higher temporal resolution than is possible using standard ASL techniques. In addition, Turbo-ASL can potentially result in higher functional sensitivity than traditional ASL techniques because of the larger number of data points acquired (5). In this work, continuous ASL (CASL) implementations of Turbo-ASL are referred to as Turbo-CASL.

For Turbo-CASL techniques, the optimum choice of the pulse repetition time (TR) depends on the arterial transit time (TT) of the label to the voxels of interest. The largest perfusion signal is seen when the TR is equal to the TT. The optimum scan timing parameters for Turbo-CASL are summarized by

$$TR = \Delta t, \quad \tau = TR - T_{acq}, \qquad [1]$$

where Δt is the ATT, τ is the tagging duration, and T_{acq} is the duration of image acquisition. This choice of $TR = \Delta t$ corresponds to the Turbo-CASL signal peak, as shown in Fig. 3 of Ref. 5. The condition on tag duration was not stated explicitly in that work, but is merely the maximum duration of tag that can be achieved while still allowing time for image acquisition. The choice of an improper TR results in a reduction in perfusion signal, which makes Turbo-CASL techniques very sensitive to TT. This brings up a number of concerns related to the Turbo-CASL signal that need to be investigated. Of primary interest is the optimization for multislice functional imaging in the presence of activation-induced TT changes.

The Turbo-CASL approach to ASL faces a couple of challenges related to its TT sensitivity. Changes in TT on the order of 100 ms have been observed upon functional activation (5–8). This means that the optimum Turbo-CASL TR differs between baseline and active states. Depending on the choice of TR, this can result in either increased or reduced sensitivity to activation, and the percentage change in signal will not necessarily reflect the true percentage change in CBF. The percentage signal change upon activation observed in traditional ASL sequences that do not use a postlabeling delay or flow-crushing gradients is also sensitive to activation-induced TT changes. However, the effect is more critical in Turbo-CASL because it affects not only the percentage signal change observed, but also the TR that should be used for the scan.

Another concern is that in sequential multislice acquisitions, each slice is acquired at a different time within the

FMRI Laboratory, Biomedical Engineering, University of Michigan, Ann Arbor, Michigan, USA.

Grant sponsor: National Institutes of Health; Grant number: DA015410; Grant sponsor: National Institute of Biomedical Imaging and Bioengineering (NBIB); Grant number: 1 R01 EB004346-01A1.

*Correspondence to: Gregory R. Lee, UM FMRI Laboratory, 2360 Bonisteel Ave., Ann Arbor, MI 48109-2108. E-mail: grlee@umich.edu

Received 24 April 2006; revised 27 October 2006; accepted 8 December 2006.

DOI 10.1002/mrm.21184
Published online in Wiley InterScience (www.interscience.wiley.com).

TR. This could lead to a variation in TT sensitivity from slice to slice. There is also a penalty to the perfusion signal amplitude as the number of slices increases. In CASL implementations, this is because the increased time spent on image acquisition means that less time is available for tagging arterial spins. A similar signal reduction occurs in pulsed ASL (PASL) implementations because the average TT to the slices of interest increases as the imaging region becomes broader. For single-coil CASL, the TTs will also increase if the labeling plane has to be moved farther from the imaging region to accommodate the additional slices.

Finally, because the Turbo-CASL sequence is optimized for a specific TT, there is varying sensitivity to perfusion over regions of different TTs. The larger the spread in TTs between regions, the less effectively Turbo-CASL will be able to image these regions simultaneously.

Aside from these concerns related to the TT sensitivity, there is a more general question concerning what the optimum TT for maximal SNR would be at a given field strength. This TT will be a compromise between the signal gained due to the increased labeling duration possible for longer TTs and the signal lost due to T_1 decay of the label during the TT. In single-coil CASL implementations, this TT is a variable that is under the experimenter's control and should be optimized. In two-coil setups, one can more easily control magnetization transfer (MT) effects, which facilitates multislice imaging. However, the physical location of the coils prevents one from changing the TT significantly.

MATERIALS AND METHODS

Simulations

We performed three simulations to investigate 1) the functional sensitivity of Turbo-CASL in the presence of activation-induced TT changes, 2) the extent of signal reduction for multislice imaging, and 3) optimization of TT (tagging plane distance) for Turbo-ASL. We performed the simulations using the analytical solution to the convolution-based Turbo-CASL model given in Eqs. [2] and [3] of Ref. 5. The relaxation parameters used were $T1_{blood} = 1.7$ s and $T1_{brain} = 1.35$ s (gray matter), which are typical values at 3T (9–11).

Simulation 1: Signal for Rest vs. Active States

To investigate the effect of activation-induced TT changes, we generated perfusion signal curves for two separate steady states (i.e., with no dynamic flow or TT changes during simulation): a baseline state (CBF = 60 ml/min/100 g, $\Delta t = 1.6$ s) and an active state with 50% larger CBF accompanied by a 150-ms (9.4%) decrease in TT. The calculated signal was plotted for a fixed TT as TR was varied. In all cases the tagging duration was set to TR − 150 ms.

For comparison, simulation of the effect of activation-induced TT changes was then repeated for a traditional ASL sequence. In this case a range of post-labeling durations within a typical 4-s TR CASL sequence was simulated for both a resting and an active state with 50% larger CBF. The percentage signal changes observed upon activation were computed.

Simulation 2: Multislice Turbo-CASL

To investigate the multislice behavior of Turbo-CASL, we performed simulations for a fixed TR of 1.6 s at a range of TTs. In this manner we determined the sensitivity of the signal to different TTs for a fixed choice of imaging sequence parameters. This is in contrast to the previous simulation, in which TT was held constant while TR and tagging duration were varied. We performed the second simulation for both a single-slice (tag duration = 1.55 s) and a nine-slice (tag duration = 1.15 s) acquisition (50 ms/slice) to compare the TT sensitivity and signal amplitudes of each acquisition.

Simulation 3: TT Optimization

In single-coil implementations, one can manipulate the TT by moving the tagging plane location. We sought to determine the optimum theoretical TT for Turbo-CASL by always choosing the optimal TR for each TT simulated (TR = Δt). Thus the TR and TT increased together, in contrast to the previous simulation in which the TR was held constant. The Turbo-CASL signal was then computed as a function of TT for both single-slice and multislice acquisitions. We converted this signal at each value of Δt to a relative measure of SNR per unit time by dividing SNR by the square root of TR.

Human Studies

Human studies were performed to complement the TT sensitivity simulations described above. To measure the dependence of the amplitude and shape of the functional response on the choice of TR, we scanned six human subjects on a 3T GE Signa LX scanner in accordance with the University of Michigan's Internal Review Board regulations. A previously described two-coil system was used to perform spin labeling (5).

The goal of the study was to measure the functional sensitivity of Turbo-CASL under different choices of TR surrounding the resting-state TT. Initially, we made a rough TT measurement by scanning each subject using the Turbo-CASL technique for six to eight equally spaced TR values between 0.8 and 2 s. Sixteen control/tag pairs were acquired at each time point for a total scan duration of 5–7 min. The tag duration was always set equal to TR minus 180 ms allotted to image acquisition. A TR with optimal signal strength (e.g., 1.4 s for subject 1) over the volume was chosen, and this TR was then assumed to be the resting-state TT. All scans used the following sequence parameters unless stated otherwise: spin echo (SE), TE = 12 ms, FOV = 20 cm, spiral readout, three adjacent 7-mm slices, and matrix size = 64 × 64.

During scanning the subjects repeated a finger-tapping paradigm six times under different imaging sequence parameters. The paradigm consisted of a 20-s rest period followed by a 10-s activation period of bilateral finger-tapping repeated 12 times to give a 6-min run. Five of these acquisitions used Turbo-CASL and one was a standard 4-s TR CASL acquisition (label duration = 3 s, postlabel delay = 0.8 s). We used the 4-s case as a control for selecting voxels to compare among the other five Turbo-CASL runs because it is not inherently biased toward a particular TT. For the Turbo-CASL acquisitions, one run was performed

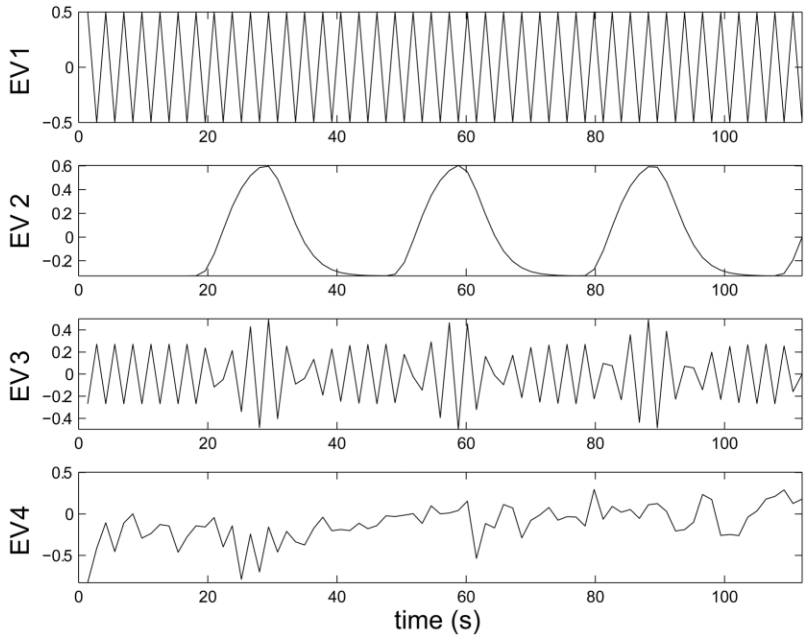

FIG. 1. EVs used in the functional analysis. From top to bottom: control/tag baseline, functional paradigm (BOLD), control/tag modulated (ASL) paradigm, and orthogonalized global mean (nuisance). The plotted EVs are from the 1.4-s run for subject 2. For clarity, only the first 80 of 258 time points are shown.

at the measured resting-state TT of the subject, and the others were performed at ±10% and ±20% of this value. As an example, the specific TRs used in the functional runs for subject 1, whose resting TT was ~1400 ms, were 1120, 1260, 1400, 1540, 1680, and 4000 ms. The order of scanning of these TRs was randomized for each subject, with the exception that the fourth scan of six was always the 4-s TR traditional CASL case.

Active voxels were determined for each scan with the use of the FMRI Expert Analysis Tool (FEAT), version 5.43, which is part of the FSL software package (FMRIB's Software Library, www.fmrib.ox.ac.uk/fsl). Before a functional analysis was performed, a global DC offset of 1000 was added to all brain voxels. A generalized least-squares analysis was carried out on unsubtracted ASL data (12). The design matrix included four explanatory variables (EVs), as diagrammed in Fig. 1. The first was a vector alternating between 0.5 and −0.5 to represent the control/tag modulation of the perfusion baseline. The second was a square wave corresponding to the experimental paradigm convolved with a gamma-variate hemodynamic response function to represent any possible BOLD signal contribution. The third EV was a control/tag modulated version of the second, and represented the desired ASL activation signal. The fourth was a nuisance regressor corresponding to the mean ASL signal within the brain to help remove artifactual global intensity fluctuations. This fourth EV was orthogonalized with respect to the other EVs to avoid penalizing true activation-related signal changes. No temporal filtering or spatial smoothing of the data was performed. A time-series statistical analysis was carried out with the use of FILM with local autocorrelation correction (13). Manual thresholding of the resulting *z*-statistic maps was used to determine active voxels. A *z*-statistic of 3.719, corresponding to an uncorrected *P*-value of 0.0001, was used as the threshold.

The results of the functional analysis were used to investigate the sensitivity and spatial localization of activation with the different TR choices. Functional time series were compared across the different Turbo-CASL acquisitions with the use of an unbiased set of voxels taken from the 4-s TR acquisition ($P < 0.0001$). We compared the sensitivity values by computing the number of voxels that were found to be active at each choice of TR. We compared the spatial location of active voxels by overlaying the individual activation maps onto an underlying perfusion image.

As an alternate measure of sensitivity, we computed the contrast-to-noise ratio (CNR) per unit time over an activation region defined as the union of the active regions for each of the six individual TRs scanned. In defining this broader activation region, we used a slightly stricter threshold of $P < 1e{-}5$. The CNR was computed as the magnitude of the ASL task regressor over the standard deviation (SD) of the residual. We then divided this value by the square root of TR to obtain a measure of CNR per unit time. Percentage ASL signal changes were also calculated over the same region. When calculating the mean and SD of the percentage signal change, we removed extreme outliers with signal changes of >500%.

RESULTS

Simulation 1

The simulated Turbo-CASL signal curves for the baseline and active states of simulation 1 are shown in Fig. 2a. It can be seen that choosing a TR near the resting-state TT results in a signal change of 41% rather than the underlying 50% perfusion change. This is due to a shift in the active-state signal curve caused by the TT reduction. Note that the largest absolute functional signal change occurs for a TR near the active-state TT of 1.45 s. The relative signal change can vary widely with the choice of TR, with a severe penalty to the functional signal if the TR is set longer than the resting-state TT. Although the baseline signal at a TR of 1.3 s in the simulation is 37% smaller than that at a TR of 4 s, the functional signal change is only

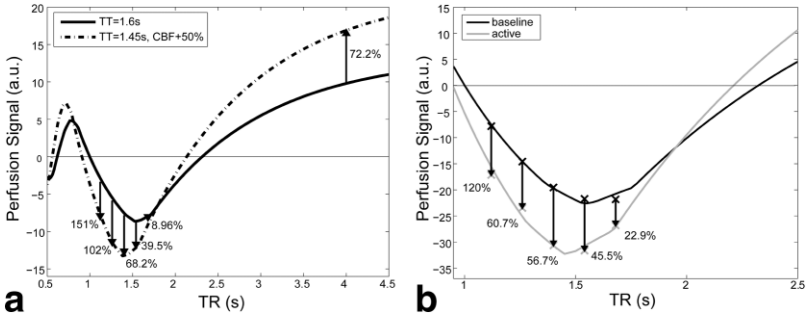

FIG. 2. **a:** Simulated signal vs. TR for two states. The baseline has $\Delta t = 1.6$ s. The active state has a 50% larger CBF and a reduced TT of 1.45 s. **b:** Measured signal for subject 1 during activation and rest at five values of TR. The curves are a fit of the Turbo-CASL model to the measured data. In both panels, numbered arrows indicate the percent signal change upon activation for various choices of TR.

15.5% smaller in amplitude. This small decrease in functional signal amplitude is more than made up for from an SNR perspective by the increased number of samples acquired. Figure 2b shows corresponding experimental data from subject 2 that show the same general pattern. These data were obtained by averaging the time-series amplitudes during both the rest and activation periods for each of the five Turbo-CASL runs. The voxels averaged were those that showed significant activation ($P < 0.0001$) in the 4-s TR case.

Simulated percentage signal changes for a standard 4-s TR acquisition at various values of the postlabeling delay, *w*, were also calculated. The postlabeling delay is defined as the time between the end of the tagging period and the start of image acquisition. For *w* shorter than the active-state TT, TT changes resulted in a substantial signal enhancement upon activation. When the postlabeling delay was 0, a 50% perfusion change accompanied by TT changes of 0, 50, 150, or 250 ms resulted in signal changes of 50%, 57%, 72%, and 87%, respectively. TT sensitivity was greatly reduced when *w* was increased to be longer than Δt. In this regime there was a small negative effect on the activation signal with TT change due to the longer T_1 of blood compared to gray matter in our simulation. TT insensitivity for values of $w > \Delta t$ was originally demonstrated for a constant flow value and TT by Alsop and Detre (14).

Simulation 2

Multislice acquisitions result in different signal behavior for each slice. It can be seen from the simulation results in Fig. 3 that the first slice is more sensitive to shorter TTs than the last. Also there is an overall reduction and broadening of the Turbo-CASL signal peak relative to a single-slice acquisition. Despite the differences, there is a significant amount of overlap between the sensitivities of the slices. It should be noted that this spread occurred for a nine-slice acquisition in which a total time of 450 ms was allotted to slice acquisition. The faster the image acquisition time, the smaller the spread in TT sensitivities and the reduction in peak Turbo-CASL signal will be.

Simulation 3

The results of simulation 3 are shown in Fig. 4. The two curves indicate the maximum perfusion signal per unit time that can be expected at each choice of TT. The curves are normalized to the peak SNR per unit time in the single-slice case. The different peaks indicate that the ideal TT for a Turbo-CASL acquisition depends on the number of slices to be scanned. For single-slice scans, the largest signal per unit time occurs for a TT of 0.65 s, although the peak is quite broad. For the five- and nine-slice acquisitions, this extends to 0.95 and 1.20 s, respectively. The amount of this extension is exactly equal to the additional amount of time spent on slice acquisition. The shaded band in the figure indicates the mean ± 1 SD of the motor cortex TTs measured in our previous work with the two-coil ASL setup (5). Keep in mind that these are the optimum TTs for Turbo-ASL type acquisitions only (timing parameters matched to Eq. [1]). For standard ASL acquisitions, it is best to keep the TT as short as possible to minimize decay of the tag during transit.

Human Studies

Representative perfusion images (subject 4) and their corresponding TT maps are shown in Fig. 5. The active voxels found in the 4-s TR case for a significance threshold of $P < 0.0001$ are displayed. These are the voxels that were subsequently used to compare the TR choices for the Turbo-CASL acquisitions in Figs. 2b and 6. In the TT maps, it can be seen that the anterior regions along the midline sup-

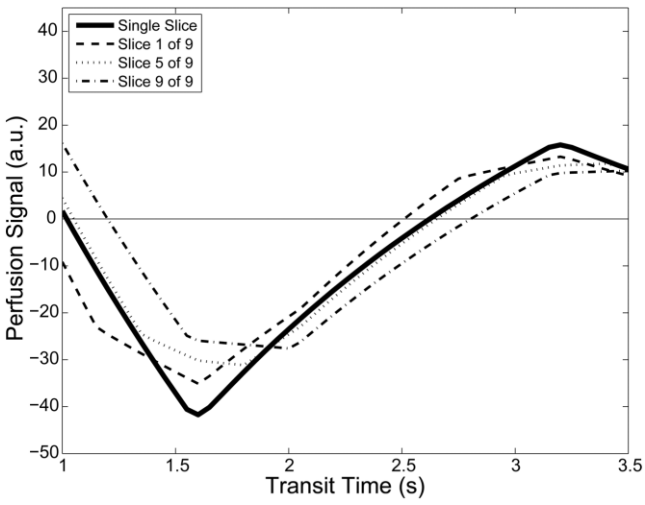

FIG. 3. Simulation of the Turbo-CASL signal at different TTs when the TR is set to a fixed value of 1.6 s. The solid black curve is an illustration of the signal for a single-slice acquisition using the same TR. The decreased time available for labeling results in signal loss for the multislice acquisition. In addition there is a slice-to-slice variation in the TT sensitivity.

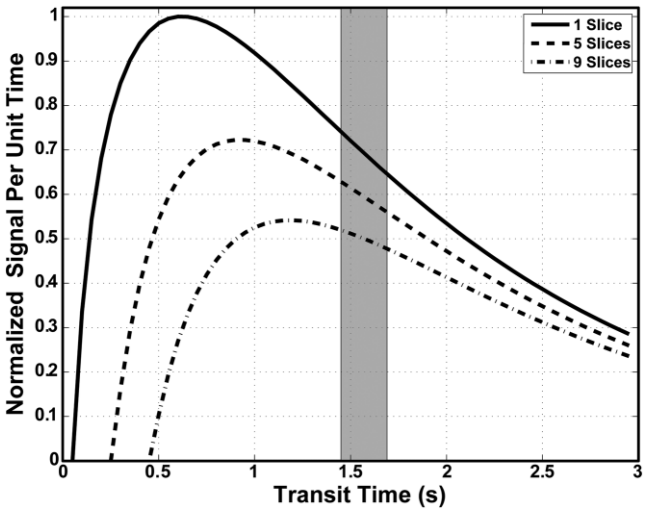

FIG. 4. Variation in the maximum achievable Turbo-CASL signal for different TTs. In all cases the TR is equal to the TT for optimal signal. This is in contrast to the simulation of Fig. 3, in which TR was held constant. The shaded region indicates typical TTs to the motor cortex for a two-coil ASL acquisition. The five- and nine-slice signal curves are normalized relative to the single-slice signal.

plied by the anterior cerebral artery have shorter TTs than the more lateral regions supplied by the middle cerebral artery. More specifically, three sample regions of interest (ROIs) are indicated for slice 3. The average gray matter TTs for regions 1, 2, and 3 are 1.12 ± 0.21, 1.42 ± 0.18, and 1.61 ± 0.14 s, respectively. Similar relative distributions of TTs among brain regions were observed for the other five subjects.

The resulting average Turbo-CASL time-series responses to activation for the active voxels of Fig. 5 are shown in Fig. 6. The voxels with TTs shorter than the baseline TR scanned are shown separately from those whose TT was longer than the baseline. In each case the trend in both baseline signal amplitudes and the amplitudes during activation agree with the trends in the simulation of Fig. 2a. For example, for the longer TT voxels, the baseline signal at the two shortest TR values is very low, but a large signal change on activation occurs. Each of the other subjects scanned showed a similar trend in baseline and activation amplitudes. The one exception was subject 5, who failed to display any active voxels at a high enough significance level in the long-TR case for a comparison across TRs to be made.

A comparison of the areas of activation detected at each TR is demonstrated by a representative slice from subject 6 in Fig. 7. The bottom right panel shows a corresponding TT map for the slice. For each TR choice, the active voxels appear to be predominantly in standard primary and supplementary motor cortex regions. The activation maps for the different TR choices largely overlap, but there are some noticeable differences. For example, the shortest Turbo-CASL TRs are more likely to show activation for regions

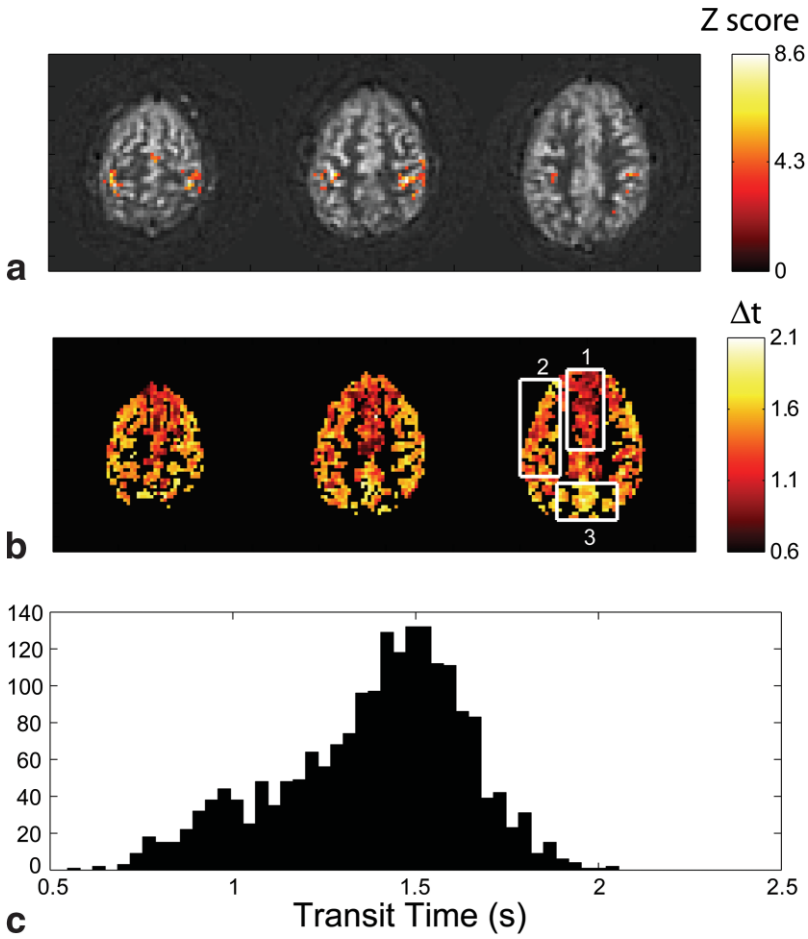

FIG. 5. Functional overlay of voxels whose *z*-statistics exceed the activation threshold onto the average perfusion image for the 4-s TR case (**a**), TT maps (**b**), and the corresponding TT histogram (**c**) for subject 2. The active voxels shown here are the ones used for subsequent comparison among the different Turbo-CASL acquisitions in Fig. 6.

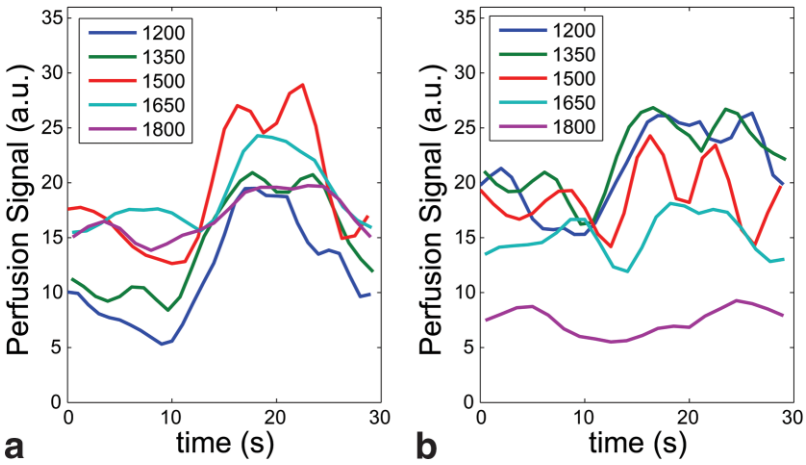

FIG. 6. Normalized average functional responses to the finger-tapping paradigm for two groups of voxels from subject 4. **a:** Long TT voxels ($\Delta t > 1.5$ s). **b:** Short TT voxels ($\Delta t < 1.5$ s). In both panels only voxels that showed activation in the 4-s TR case were used.

with shorter TTs. This can be seen for voxels around the supplementary motor cortex, which were largely below the threshold for the 1540- and 1680-ms TR values.

Table 1 lists the number of voxels that showed a significant functional signal change ($P < 0.0001$) for each choice of TR scanned. For each subject, the cell corresponding to the TR that was closest to the resting-state TT of the activating voxels in the 4-s TR case is shaded. The term "Base" in column 1 of the table refers to the baseline TR value selected from the initial Turbo-CASL imaging data as a rough estimate of the TT to the imaging region. Since the actual fitted resting-state TT of the activating motor voxels (as indicated by the shaded cells) was often somewhat longer than the initial estimate, this "Base" TR is not always the TR that was closest to the baseline TT of the motor cortex voxels. It can be seen that the acquisitions with TR shorter than the resting-state TT (shaded cell) generally show the largest number of significant voxels because at this TR the sequence is better optimized for the active state. Likewise, very few voxels are found for the longest Turbo-CASL TR choices (with the exception of subject 3). For the optimum choice of turbo-CASL TR, it can be seen that the Turbo-CASL acquisition outperformed traditional 4-s TR CASL in all but one of the subjects scanned. In practice, only a single TR choice would be used for a given study. In this case, choosing a single row corresponding to our "Base − 20%" estimate results in superior performance compared to traditional CASL in four out of six subjects.

One can construct an alternative region for comparison by taking the union of all active voxels ($P < 1e{-}5$) at the six different TR values. The CNRs per unit time over these broader regions are shown in Table 2. The highest CNR per unit time corresponds to a short TR Turbo-CASL run in five of the six subjects.

The average percentage signal changes observed upon activation for each of the scans is displayed in Table 3. As expected, the percentage signal changes observed at Turbo-CASL TR values shorter than this resting TT tend to be enhanced, while those at longer TR values are reduced (or even reversed in sign for some subjects). The SD of the percentage changes observed tends to be larger for Turbo-CASL than for standard CASL. This is to be expected, considering the TT sensitivity of the Turbo-CASL technique and the spread of TTs present within our activation region. At the shortest values of TR, baseline flow values

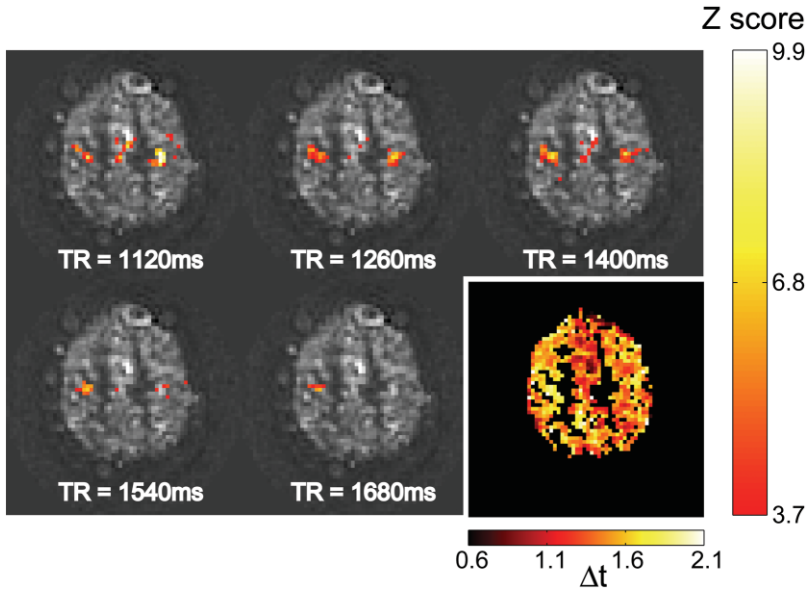

FIG. 7. Activation maps for subject 4, slice 2, for each Turbo-CASL TR used. It can be seen that while there is substantial overlap, the location of the activation detected differs somewhat. The three shorter TRs detect more activation along the midline, where TTs are shorter. The inset at the bottom right shows the corresponding TT map for reference.

Table 1
Number of Active Voxels ($P < 0.0001$)*

TR	Subject number					
	1	2	3	4	5	6
Base-20%	**63**	**112**	**191**	56	**36**	85
Base-10%	40	86	—	50	16	65
Base	40	75	65	**82**	7	74
Base+10%	13	13	29	16	0	34
Base+20%	7	0	61	7	0	15
4000 ms	27	81	73	78	9	**109**

*The TR values scanned were different for each subject. The TR listed as "Base" corresponds to the initial rough estimate of the average resting state transit time over the three slices. Base = 1400 ms for Subjects 1,2,4,6; 1300 ms for Subject 3; 1500 ms for Subject 4. Shaded cells indicate the TR closest to the actual fitted transit time of the voxels displaying significant activation. Numbers in bold indicate the TR displaying the largest number of active voxels for a given subject.

near zero can result in large percentage signal changes that can be either positive or negative.

DISCUSSION AND CONCLUSIONS

The Turbo-CASL technique is able to reliably detect activations at an improved temporal resolution and often with increased sensitivity compared to the conventional technique. The baseline signal amplitudes were lower for Turbo-CASL than for the standard CASL acquisition, but the greatly increased number of samples acquired generally resulted in a higher sensitivity corresponding to more significant voxels found by the turbo scheme for the proper choice of TR. Exaggerated percentage signal changes are observed for TRs around the active-state TT.

As predicted by simulation 1, the percentage signal changes observed for a given set of voxels was highly dependent on the choice of TR. Because of the TT decrease that occurs upon activation, it is necessary to set TR to a value less than the resting-state TT to obtain optimal Turbo-CASL signal. In theory, one could acquire a TT map both at rest and during a period of activation to measure the optimum TR for a functional experiment. This might work for tasks such as finger-tapping, but in general the active state cannot be sustained for the 10 min or so needed to acquire the TT map. In practice, setting the TR to a value approximately 200 ms below the measured resting-state TT should provide good sensitivity.

Based on the above discussion, we suggest that a typical functional imaging session should be carried out in two steps. Initially the subject should be scanned with the Turbo-CASL sequence at a range of TRs surrounding the likely TT (setting $\tau = \mathrm{TR} - T_{acq}$). The signal obtained at each of these TRs should then be fit to the analytical signal equation from Ref. 5 to determine the resting-state TT for the ROIs. In practice, a quick visual inspection of the location of the Turbo-CASL signal peak can be done instead of a fitting procedure, since high precision is not necessary at this point. This can be done in approximately 10 min at the beginning of a scanning session. For functional paradigms, the subject should be scanned at a TR that is 100–300 ms less than the measured resting-state TT value to achieve enhanced functional sensitivity.

When comparing the sensitivity of Turbo-CASL with traditional ASL, one should take the time penalty incurred by the need to acquire an initial resting-state TT map into account. The 5–10 min needed to acquire this map could be used for additional functional scanning with the traditional technique, which would result in improved sensitivity relative to that reported here. For example, scanning for 60 min instead of 50 min would result in an increase in sensitivity of nearly 10% for standard CASL. For shorter experiments this effect would become more significant, and investigators should take this into account when deciding which imaging approach to use.

The need to spend as much of the TR as possible on labeling limits the number of slices that are practical to acquire with a Turbo-CASL acquisition. For example, the simulation results predict a decrease in signal on the order of 25% when going from a one-slice to a nine-slice acquisition. Also, each individual slice within a multislice experiment has a different signal curve, as shown in Fig. 3. A TR that is optimal for one slice will not necessarily be optimal for others because of the delay between the acquisition of each slice. There is substantial overlap in slice sensitivities, and in practice, scans with a moderate number of slices are feasible. To minimize both signal loss and TT sensitivity, it is desirable to make the individual slice acquisitions as fast as possible. The current simulations assumed 50 ms/slice in the multislice acquisitions. The use of parallel imaging to further accelerate image acquisition would be beneficial with the present technique. In a

Table 2
CNR Per Unit Time Comparison (Mean ± SD) Over the Activation Region as Defined by the Union of the Activation Maps for the Six Different TRs Scanned*

TR	Subject number					
	1	2	3	4	5	6
Base-20%	0.63 ± 0.30	**0.92 ± 0.39**	1.1 ± 0.42	0.62 ± 0.32	**0.55 ± 0.21**	0.62 ± 0.28
Base-10%	**0.65 ± 0.32**	0.78 ± 0.35	—	**0.64 ± 0.28**	0.52 ± 0.27	0.54 ± 0.26
Base	0.53 ± 0.28	0.61 ± 0.37	0.60 ± 0.41	0.60 ± 0.29	0.29 ± 0.24	0.53 ± 0.23
Base+10%	0.44 ± 0.25	0.34 ± 0.27	0.42 ± 0.32	0.37 ± 0.25	0.11 ± 0.11	0.43 ± 0.29
Base+20%	0.30 ± 0.21	0.34 ± 0.27	0.48 ± 0.34	0.34 ± 0.24	0.18 ± 0.15	0.26 ± 0.21
4000 ms	0.27 ± 0.14	0.45 ± 0.21	0.42 ± 0.25	0.54 ± 0.19	0.40 ± 0.17	**0.67 ± 0.23**

*The TR values scanned were different for each subject. The TR listed as "Base" corresponds to the initial rough estimate of the average resting state transit time over the three slices. Base = 1400 ms for Subjects 1,2,4,6; 1300 ms for Subject 3; 1500 ms for Subject 4. Numbers in bold indicate the TR displaying the largest CNR per unit time for a given subject.

Table 3
Percentage Signal Change Comparison (Mean ± SD) Over the Activation Region as Defined by the Union of the Activation Maps for the Six Different TRs Scanned*

TR	Subject number					
	1	2	3	4	5	6
Base-20%	127 ± 155	147 ± 145	28.2 ± 225	99.1 ± 111	119 ± 206	60.8 ± 205
Base-10%	99.5 ± 105	113 ± 126	—	90.7 ± 93.5	90.6 ± 79.3	106 ± 140
Base	71.6 ± 68.9	90.3 ± 84.5	74.1 ± 114	82.1 ± 93.3	46.1 ± 58.1	151 ± 136
Base+10%	55.0 ± 66.8	21.7 ± 68.1	54.0 ± 87.0	48.4 ± 81.9	20.8 ± 30.1	86.7 ± 106
Base+20%	19.4 ± 43.3	−12.2 ± 60.0	71.1 ± 94.5	27.2 ± 81.5	−13.0 ± 29.3	50.6 ± 100
4000 ms	70.6 ± 59.6	85.6 ± 67.9	71.0 ± 74.5	114 ± 77	105 ± 93.7	124 ± 83.6

*The TR values scanned were different for each subject. The TR listed as "Base" corresponds to the initial rough estimate of the average resting state transit time over the three slices. Base = 1400 ms for Subjects 1,2,4,6; 1300 ms for Subject 3; 1500 ms for Subject 4.

recent CASL study, Wang et al. (15) were able to improve the SNR by using an eight-channel array coil, even at an acceleration factor of 3.

Although it is not shown explicitly in the simulation of Fig. 3, it should be noted that the percentage signal change observed upon activation can vary from slice to slice. For example, when TR is set slightly shorter than the resting-state TT, the decrease in TT upon activation typically results in a larger enhancement to the percentage signal change for the earlier slices in a multislice acquisition.

TTs are not uniform across the brain. This may preclude the use of the Turbo-CASL technique in functional scans to compare regions with significantly different TTs. Fortunately, there is a range of TTs of roughly 500 ms over which a good amount of activation signal can be observed. One can observe this by looking at the width of the region where there is significant spacing between the baseline and active-state curves in Fig. 2. Also, in some specific cases it may be possible to exploit the slice-dependent TT sensitivity of a multislice acquisition by placing the later slices toward the region of increased TT. Individual differences in baseline TT or the magnitude of the TT change observed upon activation may contribute to intersubject sensitivity differences. For the five subjects studied in this work, the mean resting TT in the ROI was 1.55 s and the SD was 0.061 s (<4%). The mean change in TT in the ROI observed upon activation was 0.102 s and the SD was 0.0431 s (42%). A larger sample is needed to determine the population variability with greater power, but the initial estimate indicates a small variability of resting TT and larger variability of the activation's effect size on TT.

From the signal curves of Fig. 4, one can see that the typical TT of around 1.5 s for a two-coil acquisition is considerably longer than would be optimal for a single-slice acquisition. On the other hand, the increased TT affords more time for multislice imaging. It should also be noted that the peaks in these curves are dependent on the T_1 relaxation rate used in the simulation. The shorter (longer) T_1 values at lower (higher) field strengths would shift these curves to the left (right) accordingly. For single-coil CASL scans, it is possible to place the inversion plane an arbitrary distance from the imaging region, and this curve can serve as a guide to the desired TT for a given number of slices. In practice, the duty-cycle limitations of our RF amplifier have precluded a single-coil implementation of Turbo-CASL because the label has to be applied every TR in order to control for MT effects. Additionally, single-coil CASL implementations suffer from reduced labeling efficiency for multislice acquisitions (16).

It should be noted that all of the simulations conducted in the present work used a CASL signal model. PASL implementations of Turbo-ASL will show very similar signal trends, but the numbers will differ somewhat due to the different form of the PASL tag delivery function.

Since flow-spoiling gradients were not used in the present work, there is a contribution from arterial blood in the activation maps for both the standard and Turbo-CASL scans. For Turbo-CASL the degree of arterial contribution will be largest for TR values closest to the TTs to the arterial vessels. In our initial experience, the use of flow spoiling extends the measured TTs (and thus the optimum TR) approximately 200–300 ms for most voxels. The TT changes that accompany activation are preserved in the presence of flow spoiling (b = 4 s/mm^2; data not shown). The added arterial contribution to the ASL signal contributes to the detection power of the measurement of activation. However, the use of flow spoilers is recommended to improve localization of the functional signal changes to the parenchymal tissue, and for experiments that require absolute quantification of perfusion. When flow-spoiling gradients are used, we expect that the active regions measured with the Turbo-CASL technique will be very similar to those found with traditional ASL techniques. The most likely source of difference would be false negatives due to reduced sensitivity in regions where the TT is longer than the chosen TR. False-positive activations should not occur for any choice of TR.

One of the attractions of functional imaging with ASL is the possibility of making a quantitative measurement. Standard ASL models will not be able to quantify the signal from a Turbo-CASL acquisition accurately because of their high sensitivity to changes in TT. Hernandez-Garcia et al. (17) recently proposed a dynamic model that can be used to quantify the signal from this type of sequence. Because the changes in TT are not measured dynamically during a scan, they suggested that a linear relationship between flow increase and TT decrease should be assumed. The validity of this assumption is currently under investigation.

The idea of an enhancement in the observed ASL signal change due to a corresponding change in TT is generally applicable to many ASL pulse sequences. It is an especially strong effect for Turbo-ASL-type sequences (either pulsed or continuous) due to the strong TT sensitivity of

the signal. Traditional ASL methods that do not use a postlabeling delay longer than the resting-state TT will experience signal enhancement as well (see simulation 1 results). This effect was observed experimentally by Gonzalez-At et al. (6). Our choice of an 800-ms postlabeling delay for the 4-s TR standard CASL comparison case falls into this signal enhancement regime. If we had used a longer postlabeling delay, the performance of the 4-s TR sequence would have been lower than that observed in the present work.

The temporal resolution for acquiring a two-coil Turbo-CASL image pair at optimal TR was between 2 and 3 s for all subjects. This is much better than the minimum of around 8 s/pair needed for substantial signal with the traditional approach. This should be of great benefit for paradigms that use short stimulation periods, such as event-related designs. In such cases the advantages of the Turbo-CASL technique relative to standard CASL are likely to be greater than those demonstrated for the 10-s duration activation block used in the present work. For studies in which accurate quantification is of primary importance, a traditional CASL sequence employing a long postlabeling delay would offer more accurate absolute CBF measurements.

A potential application of Turbo-CASL is to observe dynamic flow changes with higher temporal resolution than allowed by the traditional technique. However, one should use caution when interpreting the observed waveform shape if no correction for TT changes has been performed. When the TR is chosen to be slightly shorter than the resting-state TT, as recommended in the present work, simulations indicate that the true flow response shape will be fairly well preserved. It is mainly the amplitude of the change that is exaggerated. However, for TRs longer than or equal to the resting-state TT, a shift in TT upon activation can result in significant distortion to the response shape. This can be seen in the experimental data for TR $\geq$ 1500 ms in Fig. 6b. Initial simulation results suggest that the use of a dynamic model that incorporates TT changes will make the technique less susceptible to such errors in response shape.

The human data in the current work were obtained in a two-coil spin-labeling experiment; however, the implications for TT sensitivity apply equally well to other Turbo-ASL implementations. With the proper choice of TR, Turbo-CASL can provide enhanced functional sensitivity in the presence of activation-induced TT changes. Functional imaging studies with a modest number of slices can be carried out with improved temporal resolution and equal or improved sensitivity compared to traditional ASL approaches.

REFERENCES

1. Williams DS, Detre JA, Leigh JS, Koretsky AP. Magnetic resonance imaging of perfusion using spin inversion of arterial water. Proc Natl Acad Sci USA 1992;89:212–216.
2. Luh WM, Wong EC, Bandettini PA, Ward BD, Hyde JS. Comparison of simultaneously measured perfusion and BOLD signal increases during brain activation with T1-based tissue identification. Magn Reson Med 2000;44:137–143.
3. Aguirre GK, Detre JA, Zarahn E, Alsop DC. Experimental design and the relative sensitivity of BOLD and perfusion fMRI. Neuroimage 2002;15: 488–500.
4. Wong EC, Luh WM, Liu TT. Turbo-CASL. Arterial spin labeling with higher SNR and temporal resolution. Magn Reson Med 2000;44:511–515.
5. Hernandez-Garcia L, Lee GR, Vazquez AL, Noll DC. Fast, pseudo-continuous arterial spin labeling for functional imaging using a two-coil system. Magn Reson Med 2004;51:577–585.
6. Gonzalez-At JB, Alsop DC, Detre JA. Cerebral perfusion and arterial transit time changes during task activation determined with continuous arterial spin labeling. Magn Reson Med 2000;43:739.
7. Yang Y, Engelien W, Xu S, Gu H, Silbersweig DA, Stern E. Transit time, trailing time, and cerebral blood flow during brain activation: measurement using multislice, pulsed spin-labeling perfusion imaging. Magn Reson Med 2000;44:680–685.
8. Lee GR, Hernandez-Garcia L, Gulani V, Noll DC. Dynamic relationship between arterial transit time and perfusion and its implications for fast ASL quantification. In: Proceedings of the 14th Annual Meeting of ISMRM, Seattle, WA, USA (Abstract 2685).
9. Lu H, Clingman C, Golay X, van Zijl PCM. Determining the longitudinal relaxation time (T1) of blood at 3.0 Tesla. Magn Reson Med 2004;52: 679–682.
10. Wansapura JP, Holland SK, Dunn RS, Ball Jr WS. NMR relaxation times in the human brain at 3.0 Tesla. J Magn Reson Imaging 1999;9:531–538.
11. Zuh DC, Penn RD. Full-brain T1 mapping through inversion recovery fast spin echo imaging with time-efficient slice ordering. Magn Reson Med 2005:54:725–731.
12. Mumford JA, Hernandez-Garcia LH, Lee GR, Nichols TE. Estimation efficiency and statistical power in arterial spin labeling fMRI. Neuroimage Neuroimage 2006;33:103–114.
13. Woolrich MW, Ripley BD, Brady JM, Smith SM. Temporal autocorrelation in univariate linear modelling of FMRI data. Neuroimage 2001; 6:1370–1386.
14. Alsop DC, Detre JA. Reduced transit-time sensitivity in noninvasive magnetic resonance imaging of human cerebral blood flow. J Cereb Blood Flow Metab 1996;16:1236–1249.
15. Wang Z, Wang J, Connick TJ, Wetmore GS, Detre JA. Continuous ASL (CASL) perfusion MRI with an array coil and parallel imaging at 3T. Magn Reson Med 2005;54:732–737.
16. Alsop DC, Detre JA. Multisection cerebral blood flow MR imaging with continuous arterial spin labeling. Radiology 1998;208:410–416.
17. Hernandez-Garcia L, Lee GR, Vazquez AL, Yip CY, Noll DC. Quantification of perfusion fMRI using a numerical model of arterial spin labeling that accounts for dynamic transit time effects. Magn Reson Med 2005:54:955–964.